JACS
JOURNAL OF THE AMERICAN CHEMICAL SOCIETY
Article
pubs.acs.org/JACS

Rattle-Structured Multifunctional Nanotheranostics for Synergetic Chemo-/Radiotherapy and Simultaneous Magnetic/Luminescent Dual-Mode Imaging

Wenpei Fan,[†,⊥] Bo Shen,[‡,⊥] Wenbo Bu,*[,†] Feng Chen,[†] Kuaile Zhao,[§] Shengjian Zhang,[§] Liangping Zhou,[§] Weijun Peng,[§] Qingfeng Xiao,[†] Huaiyong Xing,[†] Jianan Liu,[†] Dalong Ni,[†] Qianjun He,[†] and Jianlin Shi*[,†]

[†]State Key Laboratory of High Performance Ceramics and Superfine Microstructures, Shanghai Institute of Ceramics, Chinese Academy of Sciences, 1295 Ding-xi Road, Shanghai 200050, P.R. China

[‡]Institute of Radiation Medicine, Fudan University, 2094 Xie-Tu Road, Shanghai 200032, P.R. China

[§]Department of Radiology, Shanghai Cancer Hospital, Fudan University, Shanghai 200032, P.R. China

Supporting Information

ABSTRACT: Most hypoxic tumors are insensitive to radiation, which is a major obstacle in the development of conventional radiotherapy for tumor treatment. Some drugs, such as cisplatin (CDDP), have been extensively used both as an anticancer drug and clinically as a radiosensitizer to enhance radiotherapy. Herein, we develop rattle-structured multifunctional up-conversion core/porous silica shell nanotheranostics (UCSNs) for delivering CDDP to tumors for synergetic chemo-/radiotherapy by CDDP radiosensitization and magnetic/luminescent dual-mode imaging. UCSNs had a dynamic light scattering diameter of 79.1 nm and excellent water dispersity and stability. *In vitro* studies showed that CDDP loaded in UCSNs (UCSNs-CDDP) was more effective than free CDDP as a radiosensitizer. After injection, UCSNs-CDDP also demonstrated unambiguously enhanced radiotherapy efficacy *in vivo*. Our report aims at presenting a novel strategy in biomedical nanotechnology that allows simultaneous dual-mode imaging and localized therapy via synergetic chemo-/radiotherapy, which may achieve optimized therapeutic efficacy in cancer treatment.

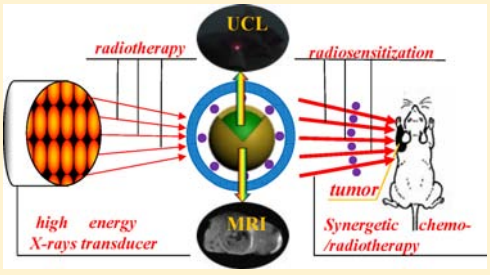

INTRODUCTION

As a representative protocol for the noninvasive treatment of cancers, radiotherapy has been widely used in clinics for decades. Theoretically, radiotherapy uses high-energy X-ray or γ-ray radiation to kill cancer cells by directly damaging DNA structure or by creating charged particles (free radicals) within the cells that can in turn break down the DNA.[1,2] More importantly, radiotherapy can force/localize almost all radiation exclusively on tumors once precisely positioned, thus reducing possible toxicity to the surrounding normal tissues. However, despite these advantages, radiotherapy may still fail to efficiently eradicate hypoxic tumors due to their insensitivity to radiation.[3−5] On the other hand, the high doses of radiation needed for tumor therapy may probably exceed the tolerance of normal cells,[6] which will inevitably cause damage to normal cells at the same time it is killing cancerous cells. Therefore, in order to enhance the sensitivity of hypoxic cells to radiation and achieve the optimal efficiency, radiosensitizers, which can enhance the effects of single or fractionated radiotherapy,[3,7] are necessary.

Recently, many high-Z materials, such as metallic nanoparticles, quantum dots (QDs), and some chemotherapy drugs, have been used as radiosensitizers to enhance the therapeutic efficiency of radiotherapy on most hypoxic tumors.[1−11] Among them, cisplatin (CDDP), an extensively used anticancer drug with favorable therapeutic activity against different kinds of cancer including neck, liver, lung, esophageal, and cervical cancers,[12] is one effective radiosensitizer that has already been applied in clinics for several years.[13−16] A number of clinical trials have shown that the administration of CDDP before radiotherapy can increase the sensitivity of hypoxic tumors to radiation as well as lower the dose of radiation needed, achieving synergy between chemotherapy and radiotherapy.[13−16] Unfortunately, in order to circumvent drug resistance, usually a high dose of free CDDP is needed, which will inevitably lead to systemic toxicity and serious pain for patients. Therefore, novel smart yet powerful drug delivery vehicles that can efficiently deliver CDDP to tumors for radiosensitization and meanwhile suppress the systemic toxicity are urgently required in the war against cancer.

Thanks to the rapid development of nanotechnology, various nano-drug carriers have come into being. Among them, rattle-type nanocapsules, which possess movable cores, porous shells,

Received: December 14, 2012
Published: April 10, 2013

   dx.doi.org/10.1021/ja312225b | J. Am. Chem. Soc. 2013, 135, 6494−6503

and interstitial hollow spaces in between, provide an attractive nanoplatform for drug delivery due to their unique hollow structure, multifunctional properties, and biological potential in the fields of nanomedicine.[17−24] In order to meet the requirements of intravenous injection by evading the reticuloendothelial systems (RES), sub-100 nm nanocapsules should be designed and fabricated; that, however, remains a major challenge, especially for nanocapsules with multilayered core/shell structures and/or multifunctionalities. Moreover, by inserting functional imaging cores (such as superparamagnetic Fe_3O_4, QDs) into the internal cavity, the nanocapsules will serve as imaging agents as well as drug vehicles, denoted as "nanotheranostics", allowing simultaneous diagnosis and in situ therapy of cancer. Despite much important progress in the synthesis of diverse nanotheranostics, no reports can be found on the use of nanotheranostics to deliver radiosensitizing drugs for synergetic chemo-/radiotherapy and simultaneous magnetic/luminescent dual-mode imaging.

Herein, multifunctional rattle-structured nanotheranostics with dual-functional up-conversion nanoparticles (UCNPs) as the core, a porous silica layer as the outer shell, and a controllable internal cavity between them have been successfully fabricated by a "surface-protected etching" strategy.[25−28] As we know, rare-earth UCNPs are considered to be promising novel fluorescent imaging probes *in vivo*,[29−31] offering unique advantages such as deep penetration, excellent photostability, relatively high brightness, and low toxicity.[32−35] Furthermore, Gd^{3+}-doped UCNPs (denoted as Gd-UCNP) can also be applied for magnetic resonance imaging (MRI), thus making them potential magnetic/luminescent dual-mode imaging probes.[35−37] In this report, we aim to design rattle-structured, multifunctional Gd-UCNP core/porous silica shell nanotheranostics (UCSNs) to achieve two major goals: (1) UCSNs could serve as a magnetic/luminescent dual-mode imaging probe for locating tumors *in vivo* based on the Gd-UCNP core, and (2) more importantly, UCSNs should be able to deliver a sufficient amount of CDDP for synergetic chemo-/radiotherapy by making use of the hollow cavity and porous shell.

EXPERIMENTAL SECTION

Cell Cytotoxicity Assessment of UCSNs. The cell cytotoxicity of UCSNs *in vitro* was evaluated by the typical 3-(4,5-dimethylthiazol-2-yl)-2,5-diphenyltetrazolium bromide (MTT) reduction assays. HeLa cells were seeded into a 96-well plate at 10^4/well and then cultured at 37 °C under 5% CO_2 for 24 h. UCSNs were dispersed into the culture media (DMEM) with different concentrations of 6.25, 12.5, 25, 50, 100, 200, 400, and 800 μg/mL and then added into the wells. After co-incubation for 12 or 24 h at 37 °C under 5% CO_2, the culture media were removed and 100 μL aliquots of MTT solution were added. After co-incubation for another 4 h, the media were replaced with 100 μL of dimethyl sulfoxide per well, and the absorbance was monitored by a microplate reader at a wavelength of 490 nm. The cell cytotoxicity was finally expressed as the percentage of cell viability relative to untreated control cells.

Magnetic Imaging *in Vitro*. HeLa cells were seeded into culture dishes at a density of 10^6/plate and then cultured for 24 h at 37 °C under 5% CO_2. After discarding old culture media, UCSNs were dispersed into DMEM solutions with different concentrations of 0, 400, and 800 μg/mL, and then added into the plate. After co-incubation for 24 h, the cells were washed three times with phosphate-buffered saline (PBS) to remove free UCSNs and detached by adding 1 mL of trypsin/EDTA. After centrifugation, the cells containing UCSNs in PBS were precipitated at the bottom of the 1.5 mL centrifuge tubes, and they were then used for MRI testes performed on a 3.0 T clinical MRI instrument.

Confocal Luminescence Imaging *in Vitro*. HeLa cells were seeded and cultured into a CLSM-special cell culture dish at 37 °C under 5% CO_2. After the cell density reached 50−60%, UCSNs were dispersed into DMEM solutions with a concentration of 200 μg/mL and then added into the culture dish. After co-incubation for 8 h, the cells were washed three times with PBS to remove free UCSNs, followed by nuclei staining by DAPI. Confocal fluorescence imaging experiments were then performed on an Olympus FV1000 laser-scanning microscope equipped with a continuous-wave (CW) near-infrared (NIR) laser at λ = 980 nm as the excitation source. A 60× oil immersion objective lens was used, and visible luminescence signals were detected in the wavelength regions of 500−560 and 620−680 nm.

Magnetic/Luminescent Dual-Mode Imaging *in Vivo*. Animal procedures were in agreement with the guidelines of the institutional Animal Care and Use Committee. Balb/c nude mice with average weight of 20 g were purchased from Laboratory Animal Center, Shanghai Medical College of Fudan University. HeLa cells (5×10^6 cells/site) were implanted subcutaneously into balb/c nude mice. Dual-mode imaging studies were performed when the tumor reached 10−12 mm average diameter (2 weeks after implant). On one hand, *in vivo* MRI tests were conducted with a 3.0 T clinical MRI instrument after intratumoral injection of UCSNs (1 mg/mL, 100 μL). *In vivo* up-conversion fluorescent imaging tests were performed using a 0−10 W adjustable 980 nm semiconductor laser (Shanghai Connet Fiber Optics, China) after intratumoral injection of UCSNs (2 mg/mL, 100 μL). Pictures were taken with a digital camera. On the other hand, after doping Tm^{3+} (1%) into Gd-UCNP ($NaYF_4$:Yb/Er/Tm@$NaGdF_4$) and conjugating folic acid (FA, targeting ligand) to UCSNs, mice were also intravenously injected with FA-UCSNs (8 mg/mL, 150 μL) for MRI tests and NIR-NIR up-conversion luminescent imaging, respectively.

CDDP Encapsulation in UCSNs. CDDP could be loaded in UCSNs by two methods. One method is simple stirring for 24 h. Briefly, predried UCSNs (10 mg) were mixed with 10 mL of CDDP solution in deionized water (1 mg/mL). After stirring for 24 h in the dark, the CDDP-loaded UCSNs nanoparticles were collected by centrifugation. To evaluate the CDDP loading capacity, the Pt concentrations of the supernatant solution and the original solution were measured by ICP-OES. The other method is vacuum impregnation, in which 10 mL of deionized water of UCSNs (1 mg/mL) was placed in a flask and then subjected to vacuum under ultrasound treatment. After 0.5 h, the vacuum pump was turned off, and 10 mL of CDDP solution in deionized water (1 mg/mL) was added dropwise. The vacuum pump was then turned on, and the process lasted for another 0.5 h. Finally, the vacuum pump was turned off, and the CDDP-loaded UCSNs particles were collected by centrifugation. Again, the Pt concentrations of the supernatant solution and the original solution were measured by ICP-OES.

CDDP Release *in Vitro*. A 10 mg portion of UCSNs was loaded into a dialysis bag (molecular weight cutoff: 3500), which was then put into the release medium (10 mL of deionized water). The system was shaken on a shaking table (170 rpm, 37 °C) in the dark. At designated time points, 3 mL samples of the solution were removed for both UV−vis and ICP-OES measurements to determine the amount of CDDP released, and then put back into the original system. Finally, the amount of CDDP released at each time point was calculated to plot the release profile.

Synergetic Chemo-/Radiotherapy *in Vitro*. HeLa cells were seeded into several six-well plates at a density of 10^5 cells/well and then cultured for 24 h at 37 °C under 5% CO_2. First, the cells were divided into five groups and exposed to different doses of radiation for 5 min: 0 (control), 2, 4, 8, and 12 Gy. The cells were then continuously cultured. All the treatments were done only once. During the next 5 days, the living cells in each group were counted, and the survival rate was calculated by dividing the number of living cells in each treated group by the number in the control group. Second, the cells were divided into seven groups: control, UCSNs, CDDP,

dx.doi.org/10.1021/ja312225b | J. Am. Chem. Soc. 2013, 135, 6494−6503

Scheme 1. Schematic Diagram of the Synthetic Procedure of UCSNs[a]

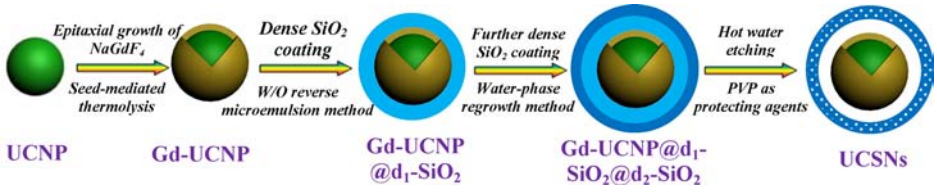

[a]Gd-UCNP was prepared through a thermal decomposition process and a seed-mediated process. Two biocompatible dense silica shells with controllable thicknesses were then coated on the as-prepared hydrophobic Gd-UCNP successively by a modified water-in-oil (W/O) reverse microemulsion method and a water-phase regrowth method. Finally, UCSNs were synthesized by a "surface-protected hot water etching" strategy to etch away the intermediate silica shell and in the meantime etch the outer dense silica shell into the porous one, yielding UCSNs with a Gd-UCNP core, a outer porous silica shell, and a hollow cavity in between.

UCSNs-CDDP, UCSNs + radiation, CDDP + radiation, UCSNs-CDDP + radiation. Briefly, 2 mL DMEM solutions of UCSNs (100 μg/mL) and CDDP/UCSNs-CDDP (2.5 μg/mL) were added into the plates and co-incubated for another 24 h. After washing away excess UCSNs and CDDP/UCSNs-CDDP three times with PBS, the cells were exposed to 2 and 4 Gy of X-ray radiation for 5 min, respectively, and then continuously cultured. All the treatments were given only once. During the next 4 days, the living cells in each group were counted, and the survival rate was calculated by dividing the number of living cells in each treated group by the number in the control group.

Synergetic Chemo-/Radiotherapy *in Vivo*. Animal procedures were in agreement with the guidelines of the institutional Animal Care and Use Committee. Balb/c nude mice with average weight of 20 g were purchased from the Laboratory Animal Center, Shanghai Medical College of Fudan University. HeLa cells (5×10^6 cell/site) were implanted subcutaneously into nude mice, which were ready for use when the tumor size reached about 0.8 cm in diameter. Some of the mice were then divided into seven groups: control, CDDP, UCSNs-CDDP, radiation, UCSNs + radiation, CDDP + radiation, and UCSNs-CDDP + radiation. Each group included six mice. Control groups received pure PBS. For synergetic therapy, UCSNs (20 mg/mL, 150 μL), CDDP (1 mg/mL, 150 μL), and UCSNs-CDDP (20 mg/mL, 150 μL) in PBS solution were directly injected into the tumors, and 0.5 h post-injection, the tumors were exposed to 8 Gy of X-ray radiation. All the treatments were given only once. During the next 2 weeks, the tumor volume of each mouse was measured by vernier caliper every other day. The other mice were divided into two groups, which were intravenously injected with FA-conjugated UCSNs-CDDP (FA-UCSNs-CDDP, 30 mg/mL, 150 μL) or free CDDP (1.5 mg/mL, 150 μL). Each group included six mice. At 3 h post-injection, the tumors were exposed to 8 Gy of X-ray radiation. The tumor volume of each mouse was also measured by vernier caliper every other day.

RESULTS

Synthesis and Characterization of UCSNs. The synthesis of UCSNs is shown in Scheme 1 and Figure 1. First, monodispersed oleate-coated $NaYF_4$:Yb/Er@$NaGdF_4$ (denoted as Gd-UCNP) was prepared through a thermal decomposition process and a seed-mediated process.[36] Second, two layers of biocompatible dense silica were coated on hydrophobic Gd-UCNP by a reverse microemulsion−water-phase regrowth method,[36,38,39] forming Gd-UCNP@d_1-SiO_2@d_2-SiO_2. Third, based on a "surface-protected hot water etching" strategy,[25−28] UCSNs were successfully synthesized with the protection of proper PVP coating, leaving an internal cavity between the Gd-UCNP core and the outer porous silica shell.

Core/shell structured Gd-UCNP was synthesized through a two-step thermal decomposition method, which could be well controlled to avoid the undesired homogeneous nucleation. As shown in Figures S1−S3, both the as-synthesized hexagonal-phase $NaYF_4$:Yb/Er (UCNP) and $NaYF_4$:Yb/Er@$NaGdF_4$ (Gd-UCNP) possess uniform spherical morphology with narrow size distributions of 24.7 ± 1.8 and 26.6 ± 1.9 nm (analysis of over 100 nanoparticles from low-magnification TEM image), respectively. The thickness of $NaGdF_4$ is roughly estimated to be around 1 nm. All the expected elements including Gd are present in Gd-UCNP, as shown by the energy-dispersive X-ray (EDX) spectrum, proving the successful coating of the $NaGdF_4$ layer. Under the excitation of a 980 nm laser, two green bands located at 519 nm ($^2H_{11/2}\rightarrow{}^4I_{15/2}$) and 538 nm ($^4S_{3/2}\rightarrow{}^4I_{15/2}$), and one red band at 651 nm ($^4F_{9/2}\rightarrow{}^4I_{15/2}$), could be observed in the emission spectrum (Figure S4). It is worth mentioning that an epitaxially grown $NaGdF_4$ layer on UCNP can not only enhance its up-conversion luminescent intensity[36,40] (Figure S4) but also serve as contrast agent in MRI.

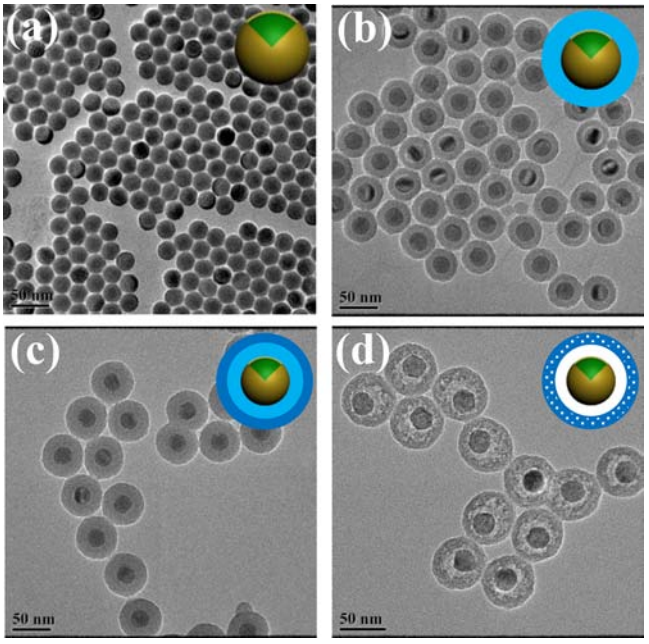

Figure 1. TEM images of (a) Gd-UCNP ($NaYF_4$:Yb/Er@$NaGdF_4$), (b) Gd-UCNP@d_1-SiO_2, (c) Gd-UCNP@d_1-SiO_2@d_2-SiO_2, and (d) UCSNs.

A biocompatible amorphous silica shell was coated on hydrophobic Gd-UCNP to give it high dispersity and stability in water through a well-established water-in-oil reverse microemulsion method, forming Gd-UCNP@d_1-SiO_2. The thickness of silica could be controlled by simply changing the amount of TEOS (Figure S5a−c), and the final silica shell

dx.doi.org/10.1021/ja312225b | J. Am. Chem. Soc. 2013, 135, 6494−6503

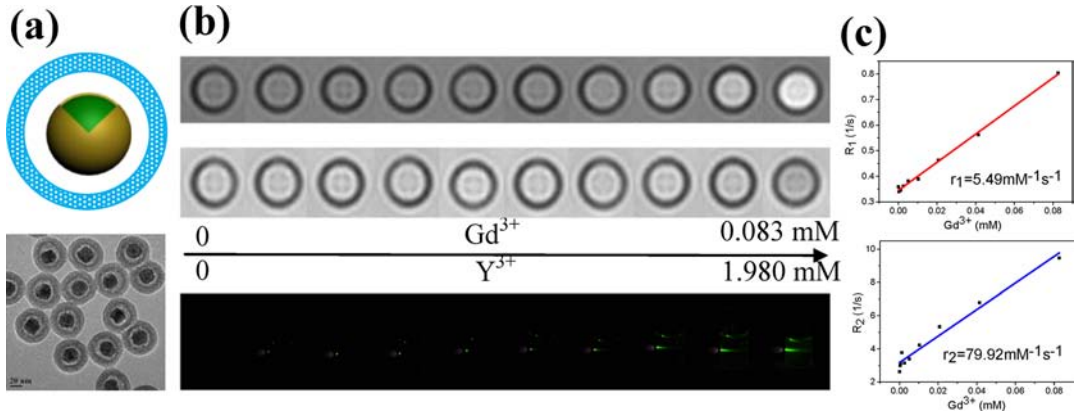

Figure 2. (a) Schematics (top) and TEM images (bottom) of UCSNs. (b) T_1- and T_2-weighted MRI maps of UCSNs with varied Gd^{3+} concentrations from 0 to 0.083 mM (top), and digital pictures of UCSNs with varied Y^{3+} concentrations from 0 to 1.980 mM (bottom). The corresponding UCSN concentration varies from 0 to 2 mg/mL. (c) Plots of R_1 (top) and R_2 (bottom) versus Gd^{3+} concentration.

thickness (d_1) of Gd-UCNP@d_1-SiO_2 was estimated to be around 10 nm (Figure 1b). A water-phase regrowth method was then adopted to quickly grow another silica shell (d_2-SiO_2) with a thickness (d_2) of 5 nm with an excess amount of ammonia as catalyst (Figure 1c). The thickness could also be precisely altered by changing the amount of TEOS (Figure S5d–f), which may contribute to optimizing its sensitivity for MRI imaging[41] and facilitate the following hot water etching.

Considering that the outer dense silica shell may prevent the permeation of most chemical molecules and limit its potential applications in many fields, such as chemical catalysis, energy storage, and drug delivery,[28] several attempts were made to turn Gd-UCNP@d_1-SiO_2@d_2-SiO_2 into rattle-type nanocapsules that could be used for drug encapsulation. Traditional alkaline-based[25−27] and acidic-based[19−21] etching methods might fail to create hollow cavities in this very thin silica shell (under 20 nm) because of the difficulty in controlling the etching rates. Fortunately, some mild etchants, such as hot water, can dissolve the colloidal silica shell by breaking the internal Si−O−Si bonds at a controllable rate to some extent, which may lead to hollow porous silica shells.

As demonstrated in Figure S6a,b, without any protection, the two dense silica shells (d_1-/d_2-SiO_2) could be etched away in hot water, because there was little structural difference between them and the outer silica was etched first followed by the second. Based on the "surface-protected etching" strategy,[25−28] biocompatible polymer PVP was chosen to protect the surface silica layer against etching. However, PVP of relatively low molecular weight (M_w = 10 000) was found not effective in protecting the outer silica layer from hot water etching, and the etching went on from the outside to the inside (Figure S6c,d). We hypothesize that high-molecular-weight polymers could stay on the surface region instead of penetrating into the shell, which is necessary for the etching protection. PVP (M_w = 40 000) was used as protecting agent here to achieve "inside-to-outside" etching. As shown in Figure S6e,f, the surface silica layer remained stable for 2 h of etching but the interior silica layer was etched out, forming a hollow cavity. Furthermore, when the etching time was extended, the cavity became ever larger, as observed in the time-dependent TEM images from the etching process (Figure S7). Continued etching for longer than 2 h might generate bigger pores in the outer silica shell, as inferred from the greater number of white blots in Figure S7e,f and the corresponding pore size distribution in Figure S8. The final UCSN products display uniform morphology and high dispersity and stability without any noticeable aggregation (Figure 1d), and the dynamic light scattering (DLS) diameter is as low as 79.1 nm (Figure S10). Moreover, some additional bands centered at about 2968 and 2950 cm^{-1} (assigned to the CH_2 stretching modes of PVP[27]) can be observed in the Fourier transform infrared (FTIR) spectra of UCSNs (Figure S11), which confirm that PVP is finally adsorbed on UCSNs, which will substantially enhance their dispersion/suspension stability in PBS solutions.

Figure 2b displays the T_1- and T_2-weighted MRI and luminescent images of UCSNs at different concentrations, and all the signals are enhanced by increasing the concentration of UCSNs. By calculation, the relaxivity values of UCSNs are estimated to be r_1 = 5.49 mM^{-1} s^{-1} and r_2 = 79.92 mM^{-1} s^{-1}, respectively (Figure 2c), which are lower thanfor Gd-UCNP@d_1-SiO_2@d_2-SiO_2 (Figure S9c), consistent with our previous results.[41] Interestingly, under the excitation of a 980 nm laser with the same power density, the emission spectrum of UCSNs shows a 2-fold enhancement in emission intensity compared to that of Gd-UCNP@d_1-SiO_2@d_2-SiO_2 (Figure 3), which could be attributed to the removal of the intermediate silica layer previously coated on Gd-UCNP after etching.[42]

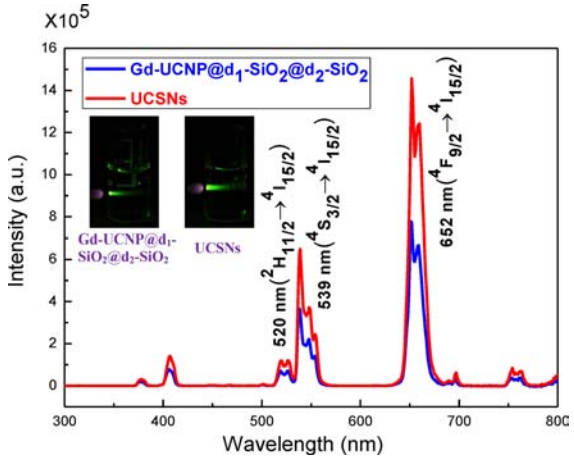

Figure 3. Up-conversion fluorescent spectra and digital photos (inset) of two samples under NIR laser excitation (λ = 980 nm): Gd-UCNP@d_1-SiO_2@d_2-SiO_2 (blue line) and UCSNs (red line). The two samples were dispersed in water at the same Y^{3+} concentration.

dx.doi.org/10.1021/ja312225b | J. Am. Chem. Soc. 2013, 135, 6494−6503

Magnetic/Luminescent Dual-Mode Imaging of UCSNs *in Vitro* and *in Vivo*. The *in vitro* biocompatibility of UCSNs was studied prior to biological experiments by a typical MTT cell viability assay. As shown in Figure S12, about 80% of the cells survived after co-incubation with 800 μg/mL UCSNs for 24 h, indicating relatively low cytotoxicity and good biocompatibility of UCSNs.

In vitro MRI of HeLa cells was investigated by co-incubation with different concentrations of UCSNs (0, 400, and 800 μg/mL) for 24 h. The cells taking up UCSNs were then precipitated at the bottom of tubes for MRI tests. As shown in Figure 4a, the MRI signal intensity gradually increases with

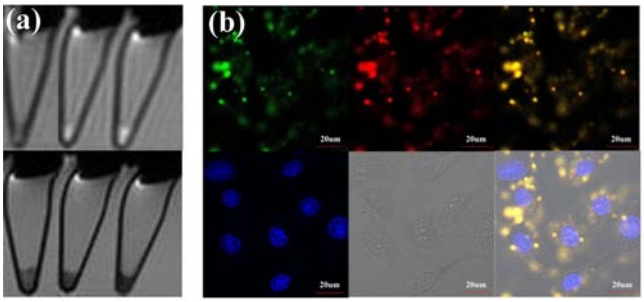

Figure 4. (a) MRI images of HeLa cells after co-incubation with UCSNs of different concentrations (from left to right: 0, 400, and 800 μg/mL) for 24 h. With increasing concentration of UCSNs added, T_1-MRI (top) and T_2-MRI (bottom) signal intensities of HeLa cells uptaking UCSNs gradually increase. (b) Confocal laser scanning microscopy (CLSM) images of HeLa cells after co-incubation with 200 μg/mL UCSNs for 8 h. The cell nucleus is stained with DAPI (blue fluorescence). Under the excitation of 980 nm light, UCSNs uptaken by the HeLa cells emit strong yellow fluorescence (merging of green and red fluorescence) in the cytoplasm of the cells, demonstrating the presence of UCSNs in the cytoplasm but not in the nucleus.

increasing concentration of UCSNs, which might be attributed to dose-dependent cellular uptake. *In vivo* MRI experiments conducted on a balb/c nude mouse using a 3.0 T human MRI scanner also display high MRI signal intensity at the tumor site after the intratumoral injection of UCSNs (Figure 5a), which demonstrates the feasibility of UCSNs as MRI contrast agents *in vivo*. We further performed the targeted *in vivo* MRI imaging

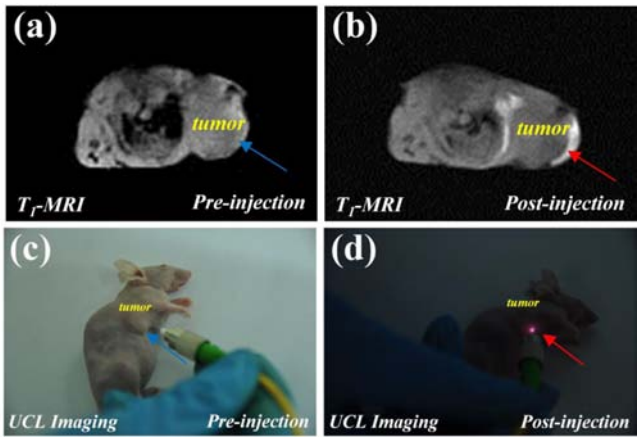

Figure 5. *In vivo* T_1-MRI (top) and up-conversion luminescent (bottom) images of a HeLa-tumor-bearing mouse before (left) and after (right) the intratumoral injection of UCSNs (2 mg/mL, 100 μL).

study by conjugating UCSNs with FA, aiming at targeting folate receptors overexpressed in HeLa tumor cells[32,46] in addition to the passive targeting arising from the enhanced permeability and retention (EPR) effects. As shown in Figure S13, both UV−vis and FTIR spectra of FA-UCSNs confirm the successful conjugation of FA onto UCSNs. After the intravenous injection of FA-UCSNs, the MRI signal intensity of HeLa tumor shows a significant increase by about 30%, 0.5 h post-injection (Figure S14), which demonstrates that FA-UCSNs were successfully delivered to HeLa tumors by active/passive targeting, resulting in enhanced MRI.

In order to observe cellular uptake of UCSNs, confocal luminescence imaging experiments were performed using an Olympus FV1000 laser-scanning confocal microscope equipped with a CW NIR laser (λ = 980 nm). As shown in Figure 4b, the HeLa cell nucleus is stained with DAPI (blue fluorescence), and strong yellow fluorescence (merging of green and red fluorescences of UCSNs under excitation by a 980 nm NIR laser) appears surrounding the cell nucleus, which implies that UCSNs have been uptaken by HeLa cells into the cytoplasm but not the cell nucleus. After the intratumoral injection of UCSNs into a balb/c nude mouse, the tumor was imaged by a 980 nm laser, and *in vivo* luminescent signal was observed under the excitation of a NIR laser (Figure 5b), demonstrating that UCSNs can also be used for luminescent imaging *in vivo*.

In order to achieve *in vivo* NIR-NIR up-conversion luminescent (UCL) imaging, Tm^{3+} (1%) was doped into Gd-UCNP, and the corresponding FA-UCSNs were injected into mice through the tail veins. As shown in Figure S15a, a bright NIR luminescent signal can be seen in tumors, demonstrating the successful accumulation of UCSNs therein by active/passive targeting.

Based on the above results, it can be concluded that UCSNs could be applied as a magnetic/luminescent dual-mode imaging probe for tumor diagnosis.

Synergetic Chemo-/Radiotherapy *in Vitro*. Using the internal cavity and porous structure on silica shell, UCSNs could be applied for storing anticancer drugs in addition to biological imaging. Here, CDDP, an extensively used clinical chemotherapy drug, was selected to be loaded into UCSNs. By quantitative measurements of Pt concentrations by ICP-OES, we found that a much higher loading capacity of CDDP (about 10 wt%) can be achieved by vacuum infusion than by simple stirring (about 5 wt%), which can be attributed to the forced infusion of CDDP molecules by the pressure difference between the outer and inside vessel, pushing more CDDP molecules into the cavity of UCSNs. As seen from the CDDP release profile in Figure S16, CDDP molecules gradually release from UCSNs over the time course, with no significant initial burst release, demonstrating that CDDP is mainly loaded into the cavity and pore channels within the shell rather than adsorbed on the outer surface of UCSNs.[12,45]

In addition to serving as a chemotherapy drug, CDDP has been applied clinically as a radiosensitizer to improve the effectiveness of radiotherapy. We conducted several *in vitro* experiments to demonstrate the enhanced efficiency of radiotherapy with CDDP (Scheme 2). First, we measured the survival rates of HeLa cells each day after exposure to different doses of radiations (calculated by comparison with a control group). As shown by radiation dose−response curves (Figure 6a), higher doses of radiation led to the survival of fewer cells, and the cells were almost totally killed when exposed to 12 Gy of radiations. During the next 5 days after the radiation, the cell

dx.doi.org/10.1021/ja312225b | J. Am. Chem. Soc. 2013, 135, 6494−6503

Scheme 2. Schematic Illustration of Radiosensitization by UCSNs-CDDP[a]

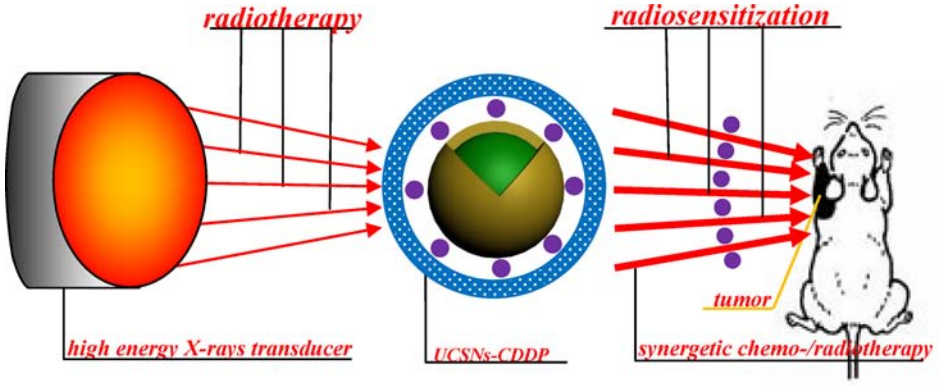

[a]When exposed to high-energy X-ray radiations, CDDP released from UCSNs can enhance the sensitivity of hypoxic tumors to radiation, thus imposing synergetic chemo-/radiotherapeutic effects on tumors growth.

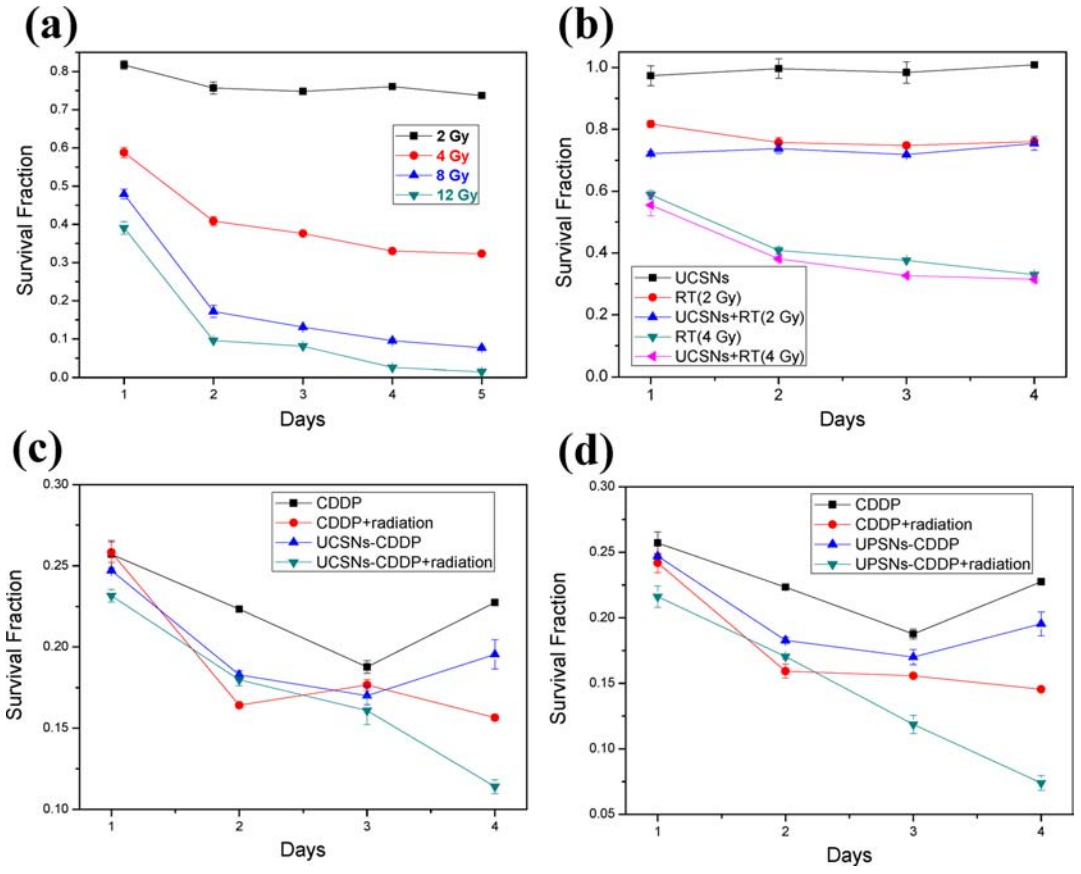

Figure 6. *In vitro* evaluation of HeLa cells with chemo-/radiotherapy. (a) Plots of fraction of HeLa cells surviving after treatment with different doses of radiation at the indicated days post-radiation. Plots of fractions of HeLa cells surviving after treatment with 100 μg/mL UCSNs in combination with 2 and 4 Gy of radiation (b), with 2.5 μg/mL free CDDP or UCSNs-CDDP in combination with 2 Gy of radiation (c), and with 2.5 μg/mL free CDDP or UCSNs-CDDP in combination with 4 Gy of radiation (d) at the indicated days post-radiation.

growth was greatly inhibited, because high-energy X-ray radiation greatly damaged the DNA structure of cancerous cells. However, high doses of X-ray radiation may also inevitably have considerable side effects on normal tissues.

Second, we studied the cytoxicity of UCSNs (100 μg/mL) on HeLa cells during the following several days. As shown in Figure 6b, the fractions of cells surviving showed no significant difference from the control group, demonstrating that UCSNs had little influence on cell growth. When exposed to 2 or 4 Gy of radiations, more cancer cells treated with UCSNs + radiation were killed than those with only radiation, which may be attributed to the contribution by the high-Z metal ions (Yb^{3+}, Gd^{3+}) in UCSNs to the radiosensitization.[3,7]

Third, we performed radiosensitization experiments by combining applications of CDDP and radiation to observe their synergetic effects in therapy. Briefly, free CDDP and loaded CDDP in UCSNs (denoted as UCSNs-CDDP) with the same concentration of 2.5 μg/mL were co-incubated with HeLa

dx.doi.org/10.1021/ja312225b | J. Am. Chem. Soc. 2013, 135, 6494−6503

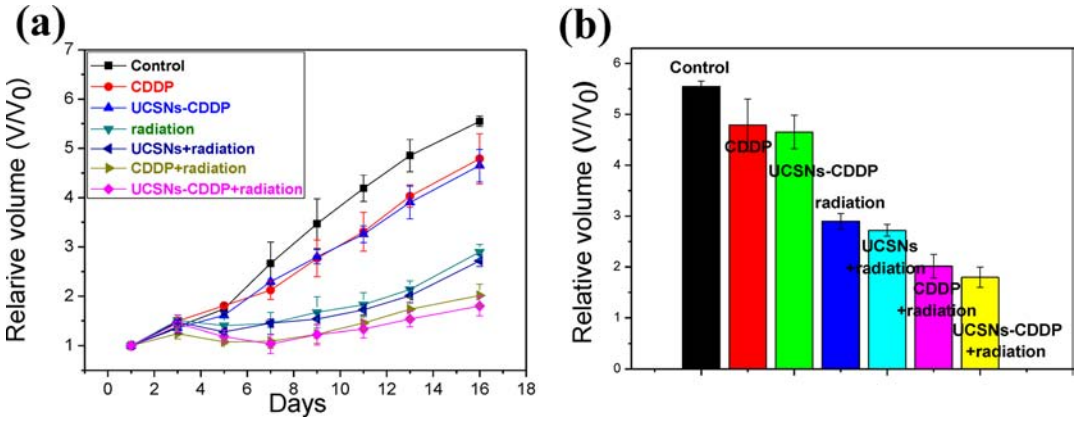

Figure 7. *In vivo* evaluation of balb/c nude mice bearing HeLa tumors treated with chemo-/radiotherapy. Mice were intratumorally injected with UCSNs, CDDP, or UCSNs-CDDP. (a) Tumor growth curves of HeLa tumor xenografts following the different treatment different modes; control groups received PBS. (b) Relative tumor volumes of mice in different treatment groups half a month after the treatments.

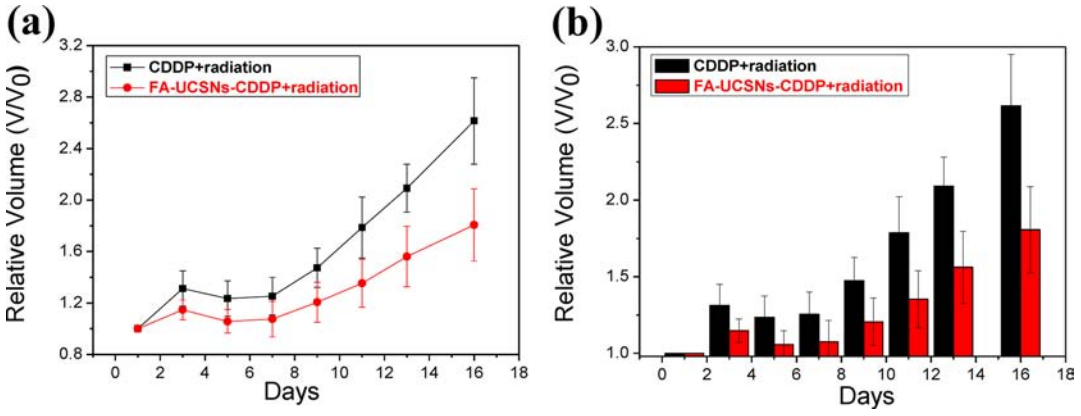

Figure 8. (a) Tumor growth curves of HeLa tumor xenografts treated with synergetic chemo-/radiotherapy. (b) Comparison between relative volumes of HeLa tumor xenografts treated with FA-UCSNs-CDDP + radiation and CDDP + radiation. Mice were intravenously injected with FA-UCSNs-CDDP and free CDDP, respectively.

cells for 24 h before radiation. As shown in Figure 6c,d, both free CDDP and UCSNs-CDDP could dramatically lower the survival rate of HeLa cells under 2 and 4 Gy of radiation, respectively, which demonstrated that CDDP could enhance the efficiency of radiotherapy under low-dose radiation. On the other hand, we found that UCSNs-CDDP exhibited higher cytoxicity and better radiosensitization than free CDDP. This phenomenon can be attributed to the gradual uptake of UCSNs-CDDP by HeLa cells through endocytosis, as compared to the passive diffusion of free CDDP. Based on the above results, UCSNs-CDDP display obvious advantages over free CDDP in radiosensitization: (1) UCSNs-CDDP can be largely uptaken by cancerous cells and CDDP released for radiosensitization. (2) The high-Z metal ions (Yb^{3+}, Gd^{3+}) also contribute to the radiosensitization. (3) UCSNs-CDDP can be expected to achieve simultaneous dual-mode imaging diagnosis and CDDP delivery for chemotherapy and enhanced radiotherapy.

Synergetic Chemo-/Radiotherapy *in Vivo*. The *in vivo* radiosensitization experiment was further conducted on balb/c nude mice bearing HeLa xenograft tumors, which were intratumorally injected with UCSNs/CDDP/UCSNs-CDDP and then subjected to high-energy X-ray radiation with a dose of 8 Gy. The tumor growth was then monitored by measuring the relative tumor volume (V/V_0) of each mouse every other day. Mice treated with PBS were used as the control group, and other six groups were those treated with CDDP, UCSNs-CDDP, radiation, UCSNs + radiation, CDDP + radiation, and UCSNs-CDDP + radiation. As shown in Figure 7a, the mice treated with CDDP and UCSNs-CDDP showed no significant difference from the control group in tumor growth, while in the mice treated with radiation and UCSNs/CDDP/UCSNs-CDDP + radiation, tumor growth was effectively inhibited in 1 week (also confirmed by digital photos in Figure S18). This indicates that radiotherapy is very effective in inhibiting tumor growth by breaking the DNA of tumor cells directly and indirectly, while chemotherapy seems less effective due to the low dose of drugs used. But in the second week post-radiation, tumors grew again due to their recovered self-reproduction capability. After half a month, we found that the mice treated with UCSNs-CDDP + radiation showed the most significant tumor growth delay and obviously higher therapy efficiency than those treated with UCSNs + radiation or with CDDP + radiation (Figure 7b), which could be attributed to the intracellular CDDP delivery and release therein from UCSNs in the tumors and the contribution of high-Z metal ions (Yb^{3+}, Gd^{3+}) in UCSNs to radiosensitization, which made hypoxic cells much more sensitive to radiation and prevented tumor cells from self-recovering, thus leading to enhanced radiotherapy effects (in coincidence with the *in vitro* therapy results in Figure 6 and H and E-stained tumor sections shown in Figure S17). The above results demonstrate that UCSNs-

dx.doi.org/10.1021/ja312225b | J. Am. Chem. Soc. 2013, 135, 6494−6503

CDDP is the most effective radiosensitizer *in vitro* and *in vivo* in the present study, and synergetic chemo-/radiotherapy effect has been achieved.

To further demonstrate the advantages of UCSNs-CDDP over free CDDP, we conjugated FA to UCSNs-CDDP for actively targeting the HeLa tumors in addition to the passive targeting, and we conducted synergetic chemo-/radiotherapy experiments by intravenously injecting FA-UCSNs-CDDP or CDDP, respectively. As shown in Figures 8 and S19, FA-UCSNs-CDDP exhibits obviously more significant tumor growth delay than free CDDP because more FA-UCSNs-CDDP was delivered to tumors via active/passive targeting effects and more CDDP molecules were released in the tumor cells, leading to enhanced radiosensitization and synergetic chemo-/radiotherapy effects in the cancer treatment.

When conducting the *in vivo* experiments by intratumoral injection of UCSNs, UCSNs mainly stayed in the tumor, and few would diffuse to other organs,[47] which could maximize the treatment efficiency and minimize the side effects. However, by intravenous injection, most UCSNs were distributed in the RES (liver, spleen, etc.).[32,48] Fortunately, by conjugating FA to UCSNs, more FA-UCSNs successfully accumulated in HeLa tumors through active ligand targeting (active targeting) and EPR effects (passive targeting), as confirmed by the *ex vivo* NIR-NIR up-conversion luminescent (UCL) imaging in Figure S15b, which could also enhance the treatment effects.

In a word, UCSNs-CDDP can be developed as a potential imaging-guided radiosensitizer in the future due to its synergetic chemo-/radiotherapy effect and its role as contrast agent in magnetic/fluorescent dual-mode imaging.

■ DISCUSSION

Cancer has been one of the most devastating diseases for many years, and the development of nanotechnology provides us with novel protocols for cancer diagnosis and therapy. Thanks to the significant progress in the synthesis of various nanostructures, multiple functionalities can be integrated into individual nanocomposite particles through different physical and chemical methods.[25] However, how to integrate the functions of multimodal imaging with varied therapeutic protocols into one kind of nanocomposite particle to accomplish simultaneous diagnostic and therapeutic functions (i.e., nanotheranostics) still remains a big challenge. Although many researchers have made substantial contributions to synthesizing various kinds of nanotheranostics and evaluating their potential clinical applications by performing experiments *in vitro* and *in vivo*,[43,45] synergetic effects among each function have been rarely considered in designing nanotheranostics. In this study, synergetic therapeutic effects, which imply significantly enhanced efficiency by the combined modalities, are reported and achieved by the interaction/promotion between two therapeutic protocols.

Radiotherapy and chemotherapy individually have been in clinical use for several decades and relieved many tumor patients of pain to a large extent. However, the optimum treatment efficiency cannot be achieved by using only one therapeutic modality. Combining the two therapeutic protocols may produce synergetically enhanced therapeutic effects. Recently, a few anticancer drugs, such as CDDP, have been used clinically for radiosensitization,[13−15] and addition of CDDP before radiation can elevate the sensitivity of most tumors to radiation and achieve synergetic treatment by combined use of chemotherapy and enhanced radiotherapy.[13] However, systemic toxicity and serious side effects may inevitably result from injecting large amounts of free CDDP and imposing high doses of radiations. The development of advanced multifunctional nanotheranostics provides a promising platform to solve these problems. In this study, we report preclinical evidence on the use of novel nanotheranostics to deliver CDDP for synergetically enhanced therapeutic effects as well as biological imaging for diagnosis and monitoring/guidance of therapeutic processes.

Such successfully fabricated multifunctional rattle-structured nanotheranostics (UCSNs) may provide an ideal nanoparticle platform for the delivery of CDDP as a radiosensitizer in addition to the synchronous dual bioimaging functions. The synthesized UCSNs exhibit uniform spherical morphology with a sharp size distribution below 100 nm and high dispersity/stability in water without any detectable aggregation, which make UCSNs an excellent drug delivery vehicle to meet the requirements of future clinical applications. Furthermore, due to the use of Gd-UCNP in the cores, UCSNs could well be used for magnetic/luminescent dual-mode imaging *in vitro* and *in vivo* (Figures 4, 5, S14, and S15). When CDDP was loaded into UCSNs, UCSNs-CDDP enhanced radiotherapy and produced synergetic therapeutic effects relative to each individual means *in vitro* and *in vivo* (Figures 6 and 7). Moreover, after the intravenous injection of FA-conjugated UCSNs-CDDP, more FA-UCSNs-CDDP accumulated in the HeLa tumor via active/passive targeting, producing much better therapeutic effects than achieved with the use of free CDDP (Figures 8 and S19). All the results reveal that UCSNs-CDDP can be developed as potential clinical radiosensitizers as well as nanotheranostics in the future.

So far, the mechanism of radiosensitization by CDDP is not completely understood. Some researchers hold the viewpoint that CDDP can prevent the replication of DNA directly and make hypoxic tumor cells combine with oxygen molecules again, which leads to enhanced sensitivity to radiation.[14] Others believe that radiation can promote the absorption of Pt by cancerous cells and elevate the combination of DNA with Pt, which enhances the killing effects of radiotherapy.[44] Despite these different views, the radiosensitization of hypoxic tumors by CDDP has been widely accepted, and synergetic therapeutic effects can be achieved by combined use of radiosensitizing chemodrugs and radiation.

The present study is the first example of synthesis of such novel multifunctional nanotheranostics that can produce unambiguous synergetic therapeutic effects of chemodrug-sensitized radiotherapy with simultaneous dual bioimaging capability. We expect that this study will shed light on the possible design and synthesis of other kinds of radiosensitization-based multifunctional nanotheranostics. Of course, there is a long way to go before realizing clinical use of the designed nanotheranostics.

■ CONCLUSION

In this work, we have introduced nanotechnology into noninvasive high-energy X-ray radiotherapy by fabricating rattle-structured up-conversion core/porous silica shell nanotheranostics (UCSNs) with a Gd-UCNP core, a porous silica shell, and a hollow cavity in between. The nanotheranostics act as a carrier of anticancer drug (CDDP) to achieve synergetic chemo-/radiotherapy by chemodrug-sensitized radiotherapy as well as *in situ* simultaneous magnetic/fluorescent dual-mode imaging. The as-synthesized UCSNs show excellent water

dx.doi.org/10.1021/ja312225b | J. Am. Chem. Soc. 2013, 135, 6494−6503

dispersity and biocompatibility after PVP coating on their outer surface. CDDP-loaded UCSNs (UCSNs-CDDP) demonstrate highly effective endocytosis by cancerous cells (shown by confocal fluorescent image) and enhanced radiosensitizing efficiency compared to free CDDP (shown by *in vitro* and *in vivo* studies of chemo-/radiotherapy). *In vivo* experiments on balb/c nude mice bearing HeLa tumors further demonstrate that UCSNs-CDDP can synergetically combine chemotherapy and radiotherapy to provide higher therapeutic efficacy than the individual therapeutic protocols. We also anticipate that the unique structure of UCSNs can be similarly employed to incorporate other kinds of sensitizers or enhancement agents (such as photosensitizers, ultrasound enhancement agents, and thermosensitizers) for the treatment of malignant tumors by varied bimodal or even trimodal (e.g., photodynamic/chemo/radio) therapeutic strategies under synchronous imaging monitoring/guidance.

■ ASSOCIATED CONTENT

Ⓢ Supporting Information

Synthetic procedures for Gd-UCNP, Gd-UCNP@d_1-SiO_2, Gd-UCNP@d_1-SiO_2@d_2-SiO_2, UCSNs, and FA-UCSNs, materials, characterizations, and other supplementary figures. This material is available free of charge via the Internet at http://pubs.acs.org.

■ AUTHOR INFORMATION

Corresponding Author

jlshi@sunm.shcnc.ac.cn; wbbu@mail.sic.ac.cn

Author Contributions

⊥W.F. and B.S. contributed equally to this work.

Notes

The authors declare no competing financial interest.

■ ACKNOWLEDGMENTS

This work has been financially supported by the National Natural Science Foundation of China (Grant Nos. 50823007, 50972154, 51132009, 51072212, 21172043, 51102259), the Shanghai Rising-Star Program (Grant No. 12QH1402500), the Nano special program of the Science and Technology Commission of Shanghai (Grant No. 11nm0505000), the Development Foundation for Talents of Shanghai (Grant No. 2012035), the National Basic Research Program of China (973 Program, Grant No. 2011CB707905), and the China National Funds for Distinguished Young Scientists (51225202).

■ REFERENCES

(1) Sauré, A.; Patrick, J.; Tyldesley, S.; Puterman, M. L. *Eur. J. Oper. Res.* **2012**, *223*, 573.

(2) Mitrasinovic, P. M.; Mihajlovic, M. L. *Curr. Radiopharm.* **2008**, *1*, 22.

(3) Hainfeld, J. F.; Dilmanian, F. A.; Slatkin, D. N.; Smilowitz, H. M. *J. Pharm. Pharmacol.* **2008**, *60*, 977.

(4) Nakae, T.; Uto, Y.; Tanaka, M.; Shibata, H.; Nakata, E.; Tominaga, M.; Maezawa, H.; Hashimoto, T.; Kirk, K. L.; Nagasawa, H.; Hori, H. *Bioorg. Med. Chem.* **2008**, *16*, 675.

(5) Ridder, M. D.; Esch, G. V.; Engels, B.; Verovski, V.; Storme, G. *Bull. Cancer* **2008**, *95*, 282.

(6) Takahashi, J.; Misawa, M. *NanoBiotechnology* **2008**, *3*, 116.

(7) Juzenas, P.; Chen, W.; Sun, Y.-P.; Coelho, M. A. N.; Generalov, R.; Generalova, N.; Christensen, I. L. *Adv. Drug Delivery Rev.* **2008**, *60*, 1600.

(8) Takahashi, J.; Misawa, M. *Radiat. Phys. Chem.* **2009**, *78*, 889.

(9) Misawa, M.; Takahashi, J. *Nanomedicine: Nanotechnol., Biol. Med.* **2011**, *7*, 604.

(10) David Gara, P. M.; Garabano, N. I.; Llansola Portoles, M. J.; Moreno, M. S.; Dodat, D.; Casas, O. R.; Gonzalez, M. C.; Kotler, M. L. *J. Nanopart. Res.* **2012**, *14*, 741.

(11) Gudkov, S. V.; Garmash, S. A.; Shtarkman, I. N.; Chernikov, A. V.; Karp, O. E.; Bruskov, V. I. *Dokl. Biochem. Biophys.* **2010**, *430*, 1.

(12) Gu, J.; Su, S.; Li, Y.; He, Q.; Zhong, J.; Shi, J. *J. Phys. Chem. C* **2010**, *1*, 3446.

(13) Marshall, N. E.; Ballman, K. V.; Michalak, J. C.; Schomberg, P. J.; Burton, G. V.; Sandler, H. M.; Cascino, T. L.; Jaeckle, K. A.; Buckner, J. C. *J. Neuro-Oncol.* **2005**, *77*, 315.

(14) Cakir, S.; Egehan, I. *Lung Cancer* **2004**, *43*, 309.

(15) Forastiere, A. A.; Goepfert, H.; Maor, M.; Pajak, T. F.; Weber, R.; Morrison, W.; Glisson, B.; Trotti, A.; Ridge, J. A.; Chao, C.; Peters, G.; Lee, D.-J.; Leaf, A.; Ensley, J.; Cooper, J. *New Engl. J. Med.* **2003**, *349*, 2091.

(16) Lagrang, J.-L.; Bondlau, P.-Y.; Tessier, E.; Chacvel, P.; Renee, N.; Etienee, M.-C.; Mllano, G. *Int. J. Cancer* **1996**, *68*, 452.

(17) Li, Y.; Shi, J.; Hua, Zile; Chen, H.; Ruan, M.; Yan, D. *Nano Lett.* **2003**, *3*, 309.

(18) Zhao, W.; Chen, H.; Li, Y.; Li, L.; Lang, M.; Shi, J. *Adv. Funct. Mater.* **2008**, *18*, 2780.

(19) Chen, D.; Li, L.; Tang, F.; Qi, S. *Adv. Mater.* **2009**, *21*, 3804.

(20) Tan, L.; Chen, D.; Liu, H.; Tang, F. *Adv. Mater.* **2010**, *22*, 4885.

(21) Li, L.; Tang, F.; Liu, H.; Liu, T.; Hao, N.; Chen, D.; Teng, X.; He, J. *ACS Nano* **2010**, *4*, 6874.

(22) Chen, Y.; Chen, H.; Guo, L.; He, Q.; Chen, F.; Zhou, J.; Feng, J.; Shi, J. *ACS Nano* **2010**, *4*, 529.

(23) Chen, Y.; Chu, C.; Zhou, Y.; Ru, Y.; Chen, H.; Chen, F.; He, Q.; Zhang, Y.; Zhang, L.; Shi, J. *Small* **2011**, *7*, 2935.

(24) Chen, Y.; Chen, H.; Sun, Y.; Zheng, Y.; Zeng, D.; Li, F.; Zhang, S.; Wang, X.; Zhang, K.; Ma, M.; He, Q.; Zhang, L.; Shi, J. *Angew. Chem., Int. Ed.* **2011**, *50*, 12505.

(25) Zhang, Q.; Ge, J.; Goebl, J.; Hu, Y.; Lu, Z.; Yin, Y. *Nano Res.* **2010**, *2*, 583.

(26) Zhang, Q.; Lee, I.; Ge, J.; Zaera, F.; Yin, Y. *Adv. Funct. Mater.* **2010**, *20*, 2201.

(27) Zhang, Q.; Zhang, T.; Ge, J.; Yin, Y. *Nano Lett.* **2008**, *8*, 2867.

(28) Hu, Y.; Zhang, Q.; Goebl, J.; Zhang, T.; Yin, Y. *Phys. Chem. Chem. Phys.* **2010**, *12*, 11836.

(29) Chatterjee, D. K.; Gnanasammandhan, M. K.; Zhang, Y. *Small* **2010**, *6*, 2781.

(30) Wang, C.; Tao, H.; Cheng, L.; Liu, Z. *Biomaterials* **2011**, *32*, 6145.

(31) Wang, F.; Han, Y.; Lim, C. S.; Lu, Y.; Wang, J.; Xu, J.; Chen, H.; Zhang, C.; Hong, M.; Liu, X. *Nature* **2010**, *463*, 1061.

(32) Xiong, L.-Q.; Chen, Z.-G.; Yu, M.-X.; Li, F.-Y.; Liu, C.; Huang, C.-H. *Biomaterials* **2009**, *30*, 5592.

(33) Cao, T.; Yang, Y.; Gao, Y.; Zhou, J.; Li, Z.; Li, F. *Biomaterials* **2011**, *32*, 2959.

(34) Zhou, J.; Liu, Z.; Li, F. *Chem. Soc. Rev.* **2012**, *41*, 1323.

(35) Liu, J.; Bu, W.; Zhang, S.; Chen, F.; Xing, H.; Pan, L.; Zhou, L.; Peng, W.; Shi, J. *Chem.—Eur. J.* **2012**, *18*, 2335.

(36) Chen, F.; Bu, W.; Zhang, S.; Liu, X.; Liu, J.; Xing, H.; Xiao, Q.; Zhou, L.; Peng, W.; Wang, L.; Shi, J. *Adv. Funct. Mater.* **2011**, *21*, 4285.

(37) Wang, F.; Deng, R.; Wang, J.; Wang, Q.; Han, Y.; Zhu, H.; Chen, X.; Liu, X. *Nat. Mater.* **2011**, *10*, 968.

(38) Xing, H.; Bu, W.; Zhang, S.; Zheng, X.; Li, M.; Chen, F.; He, Q.; Zhou, L.; Peng, W.; Hua, Y.; Shi, J. *Biomaterials* **2012**, *33*, 1079.

(39) Chen, F.; Zhang, S.; Bu, W.; Liu, X.; Chen, Y.; He, Q.; Zhu, M.; Zhang, L.; Zhou, L.; Peng, W.; Shi, J. *Chem.—Eur. J.* **2010**, *16*, 11254.

(40) Guo, H.; Li, Z.; Qian, H.; Hu, Y.; Muhammad, I. N. *Nanotechnology* **2010**, *21*, 125602.

(41) Chen, F.; Bu, W.; Zhang, S.; Liu, J.; Fan, W.; Zhou, L.; Peng, W.; Shi, J. *Adv. Funct. Mater.* **2013**, *23*, 298.

(42) Li, Z.; Zhang, Y.; Jiang, S. *Adv. Mater.* **2008**, *20*, 4765.

(43) Chen, Y.; Chen, H.; Zeng, D.; Tian, Y.; Chen, F.; Feng, J.; Shi, J. *ACS Nano* **2010**, *4*, 6001.

(44) Peters, W. A.; Liu, P. Y.; Barrett, R. J.; Stock, R. J.; Monk, B. J.; Berek, J. S.; Souhami, L.; Grigsby, P.; Gordon, W.; Alberts, D. S. *Clin. Oncol.* **2000**, *18*, 1606.
(45) Chen, Y.; Gao, Y.; Chen, H.; Zeng, D.; Li, Y.; Zheng, Y.; Li, F.; Ji, X.; Wang, X.; Chen, F.; He, Q.; Zhang, L.; Shi, J. *Adv. Funct. Mater.* **2012**, *22*, 1586.
(46) Wu, H.; Liu, G.; Zhang, S.; Shi, J.; Zhang, L.; Chen, Y.; Chen, F.; Chen, H. *J. Mater. Chem.* **2011**, *21*, 3037.
(47) Idris, N. M.; Gnanasammandhan, M. K.; Zhang, J.; Ho, P. C.; Mahendran, R.; Zhang, Y. *Nat. Med.* **2012**, *18*, 1580.
(48) Cui, S.; Yin, D.; Chen, Y.; Di, Y.; Chen, H.; Ma, Y.; Achilefu, S.; Gu, Y. *ACS Nano* **2013**, *7*, 676.